Voltage- and Flow-Controlled Electrodialysis Batch Operation: Flexible and Optimized Brackish Water Desalination

Wei He[a,b,1,*], Anne-Claire Le Henaff[a,1], Susan Amrose[a], Tonio Buonassisi[a], Ian Marius Peters[a], Amos G. Winter, V[a]

[a]*Department of Mechanical Engineering, Massachusetts Institute of Technology, Cambridge, MA, 02139, United States*
[b]*School of Engineering, University of Warwick, Coventry, CV4 7AL, United Kingdom*

Abstract

Electrodialysis (ED) desalination has been demonstrated to be more energy-efficient, provide higher-recovery, and be lower-cost for producing drinking water from saline groundwater compared to reverse osmosis. These benefits of ED could translate into cost-effective, renewable-powered desalination solutions. However, the challenge of using a variable power source (e.g. solar) with traditional steady-state ED operation requires batteries to reshape the power source to match the desalination load; these batteries often contribute to a large fraction of the produced water cost. In this study, we propose a time-variant voltage- and flow-controlled ED operation that can enable highly flexible desalination from variable power sources, including renewables, with negligible batteries, potentially leading to reduced water costs compared to what existing technology can provide. A model-based controller is presented which varies applied ED stack voltage and pumping flow rate to match power consumption to a variable source while maximizing desalination rate throughout an ED batch. The utility of the controller was demonstrated with a pilot-scale system tested with brackish groundwater, which operated as expected under varying fixed power levels and a real solar irradiance profile. The pilot system achieved a production rate up to 45% higher than that of an equivalently sized traditional steady-state ED system.

Keywords:
Brackish Water Desalination, Variable Power, Electrodialysis, Variable Voltage and Flow, Model-Based Control

1. Introduction

1.1. Background

Almost two-thirds of the world's population, approximately four billion people, face severe water scarcity during at least one month of the year [1]. Pressures from population growth and climate change are expected to exacerbate this water stress by increasing water demand as water supplies become more erratic and uncertain [2]. One approach to mitigate water stress is to make use of brackish groundwater, or groundwater with a total dissolved solids (TDS) concentration above the taste threshold (>500 mg/L). Brackish groundwater is prevalent throughout the world [3, 4, 5] and is increasingly being used in the Middle East and North Africa to meet municipal water demand [6]. However, its use is limited by the high-cost of desalination, difficulties of managing large volumes of waste brine, and the high costs of integrating with off-grid energy sources [7]. These issues are most challenging in remote, off-grid, rural communities that are prevalent in countries such as India [8], where the majority of those facing severe water scarcity live [1].

Currently, the dominant method of desalinating brackish groundwater is reverse osmosis (RO) [9]. Wright et al. demonstrated that photovoltaic (PV)-powered electrodialysis (ED) can be an energy- and cost-effective alternative solution to RO for village-scale applications, particularly suited to rural India [8]. ED has a lower energy consumption per unit water produced compared to RO (75% less at 1,000 mg/L and 30% less at 3,000 mg/L), and a greater water recovery ratio (nearly double that of current village-scale RO systems) [8]. The high energy efficiency of ED reduces its carbon footprint and translates into a smaller, less expensive renewable power systems than those required for off-grid RO, which could reduce total water costs. The high water recovery could

*Corresponding a author
Email address: whe@mit.edu, Wei.He.2@warwick.ac.uk (Wei He)
[1]Shared first authorship

also lower water wastage and brine management costs relative to RO. These combined features make ED a promising technology for cost-constrained communities in developing countries and water scarce regions [10].

Although ED is amenable to renewable power due to its low specific energy consumption for brackish water desalination, remaining challenges arise from balancing variable renewable power sources and electrical demand for producing water. A traditional static ED system typically operates at a constant voltage and flow rate, which creates an inflexible electrical load that often requires large battery banks to reshape the variable power input (from a source such as solar) for meeting the desalination demand throughout the day. As a result, batteries contribute a large fraction of the lifetime cost and the total water cost for an off-grid ED system [11, 12, 13]. Similar challenges are also faced ED systems powered by electrical grids with incorporated wind and solar sources; to constantly meet electrical demands (including desalination), high-cost energy storage is essential to provide the flexibility that cancels out the intermittence of the renewables [14, 15].

1.2. Benefits of time-variant desalination

To mitigate some of these challenges and costs associated with energy storage, this study proposes a time-variant ED operation by varying voltage and flow rate, to catalyse the flexible use of variable power sources with negligible batteries. Using the proposed flexible operation, these time-variant ED systems could produce more water than demanded when excess power is available (say on sunny time) and store it for periods when power is not available (say on cloudy time); this approach would effectively store energy as treated water, rather than storing it in batteries [13]. The flexibility in utilizing variable power for water production could reduce battery capacity compared to that required by traditional renewable energy-powered ED systems that have similar daily production rates, thereby potentially reducing total water costs.

Flexible desalination operation also offers several benefits to on-grid desalination. It could enable the exploitation of variable electricity tariffs (particularly low tariffs during off-peak times) to reduce energy costs for desalination, as off-peak electricity tariffs are often less expensive than peak electricity tariffs [16]. Flexible desalination can also aid in lowering costs and carbon emissions of the electrical grid, as the flexible ED operation could help smooth intermittent renewable power and lead to less energy storage required for the supply-demand balance.

1.3. Review of prior work

Several flexible operation strategies for desalination have previously been explored for minimizing required energy storage. Richards et al. [17] presented a flexible RO brackish water desalination system under an established safe operating window constrained by operational variables, in which the system could directly utilize wind or solar power sources to continuously produce water without batteries. This flexible RO theory was later experimentally demonstrated to produce water under wind power at various speeds [18] and solar power at several irradiance levels [19]. These studies indicate that it is technically feasible to operate RO systems powered by renewable energy sources such as solar or wind, but highly fluctuating variable sources may lead to reduced production rates [20, 21]. Cirez et al. [22] developed a flexible PV-ED system using an optimized PV module design, which was composed of multiple connected PV cells in series/parallel that could vary voltage applied to the ED stack and maximize energy transfer given available solar irradiance. Malek et al. [23] demonstrated robust and stable desalination performance in a lab-scale, directly-coupled, wind-powered ED system under various wind speeds, turbulence intensities, and periods of oscillation. The study indicated that specific energy consumption of the process was relatively unaffected by fluctuations tested in the lab-scale wind-ED system [21]. Veza et al. [24] actively controlled the flow rate and voltage of a wind-powered ED system by developing a database of correlations between available energy, product concentration, flow rate, and voltage applied to the two ED stacks in the system. The coordinated flow rate and product water conductivity by the developed controller based on the database enable the ED unit to adapt smoothly to variations in wind power, even when sudden drops/rises occurred [25]. Recently, Xu et al. [26] experimentally tested a small-scale PV-ED system under three different solar conditions (i.e. sunny, cloudy, and overcast days) with predefined operations that were fixed in each day. Their results indicated that higher flow rates and better solar irradiance can lead to higher production rates of the ED system [26]. Campione et al. [27] used transitory simulation models to numerically investigate ED's performance at two different time scales and indicated the suitability of ED for the integration with polygeneration systems as an energy-buffer.

Each of these systems adjusted water production rates to maximize utilization of the variable power resource. However, none of these prior studies presents a deterministic model for how to control the voltage and flow rate of an ED system to utilize all available power from a

variable power source while maximizing water production rate. In water-stressed, cost-constrained settings, the utility of maximizing production is to increase the number of people who can gain access to potable water. Furthermore, maximizing water production from a finite system size can lead to smaller, lower-cost ED systems by improving the productivity per unit material (e.g. membranes).

1.4. Objectives of this study

The objective of the present study is to develop and demonstrate a highly-flexible, time-variant ED operation strategy that can accommodate variable power sources. This work is built on our previous research focused on PV-ED system cost optimization with a flexible on-off control strategy proposed by Bian et al.[13], which maximizes utilization of solar power on a day-by-day basis to reduce required battery capacity, and a voltage controlled strategy proposed by Shah et al. [28], which maximizes water production rate by continuously changing the voltage applied to an ED stack to operate near limiting current density throughout a batch. In the present study, by introducing a new degree of freedom in control – flow rate – the proposed flexible ED operation can simultaneously maximize drinking water production and variable power utilization. This is achieved by actively optimizing and controlling the voltage applied to an ED stack and the flow rate through it. To create, validate, and explore this highly-flexible ED technology, this paper we:

1. codify the flexibility of batch ED operation given voltage- and flow-controlled operation, and their impact on water production;
2. develop a model-based controller that simultaneously co-maximizes water production rate and variable power utilization; and
3. validate the controller using a pilot-scale time-variant ED system and benchmark its performance relative to conventional static ED operation.

2. Electrodialysis desalination and time-variant operation

2.1. Electrodialysis desalination

ED is an electrochemical process that removes ions using an external electric field with selective ion-exchange membranes. In an ED system (Fig. 1), saline water flows through an ED stack which contains a series of alternating anion exchange membranes (AEM) and cation exchange membranes (CEM). AEMs only allow passage of anions and CEMs only pass cations. With an electric field applied over the ED stack, anions flow towards the anode and cations towards the cathode. Therefore, the placement of AEMs and CEMs in series selectively controls the ion removal across the membranes, and produces alternating channels of diluate and concentrate.

Basic ED operation is usually classified as: continuous operation, in which a saline feed is desalinated within a single pass through multiple ED stages (Fig. 1a); and batch operation, in which diluate and concentrate are recirculated through a single-stage ED stack until the diluate is desalinated to a desired product concentration (Fig. 1b). There are also other ED operations that hybridize continuous and batch operations, such as feed and bleed [29, 30], that combine their advantages. Compared to continuous ED, batch ED potentially requires a smaller stack, a smaller footprint, less membrane area, and lower capital costs to build a small-scale desalination system [13, 31, 28]. Based on these advantages, this study focuses on batch ED operation.

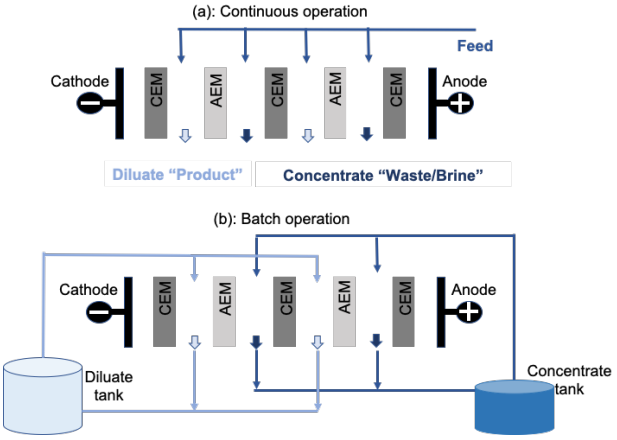

Figure 1: Schematic of ED desalination operation. In ED, an electric field is applied across alternating cation (CEM) and anion (AEM) exchange membranes to transport ions from the diluate channels to the concentrate channels. In a continuous ED system (a), feed is often passed through multiple ED stacks to produce product water. In an batch ED system (b), diluate and concentrate are recirculated through a single ED stack until the diluate is desalinated to a desired product concentration.

2.2. The concept and advantages of voltage- and flow-controlled ED operation

Figure 2 illustrates the advantages of voltage- and flow-controlled ED operation, namely through improved operational flexibility and water production compared to conventional static ED operation and voltage-controlled ED operation. The term “flexibility" in this study refers to the variability of power at which the ED system is

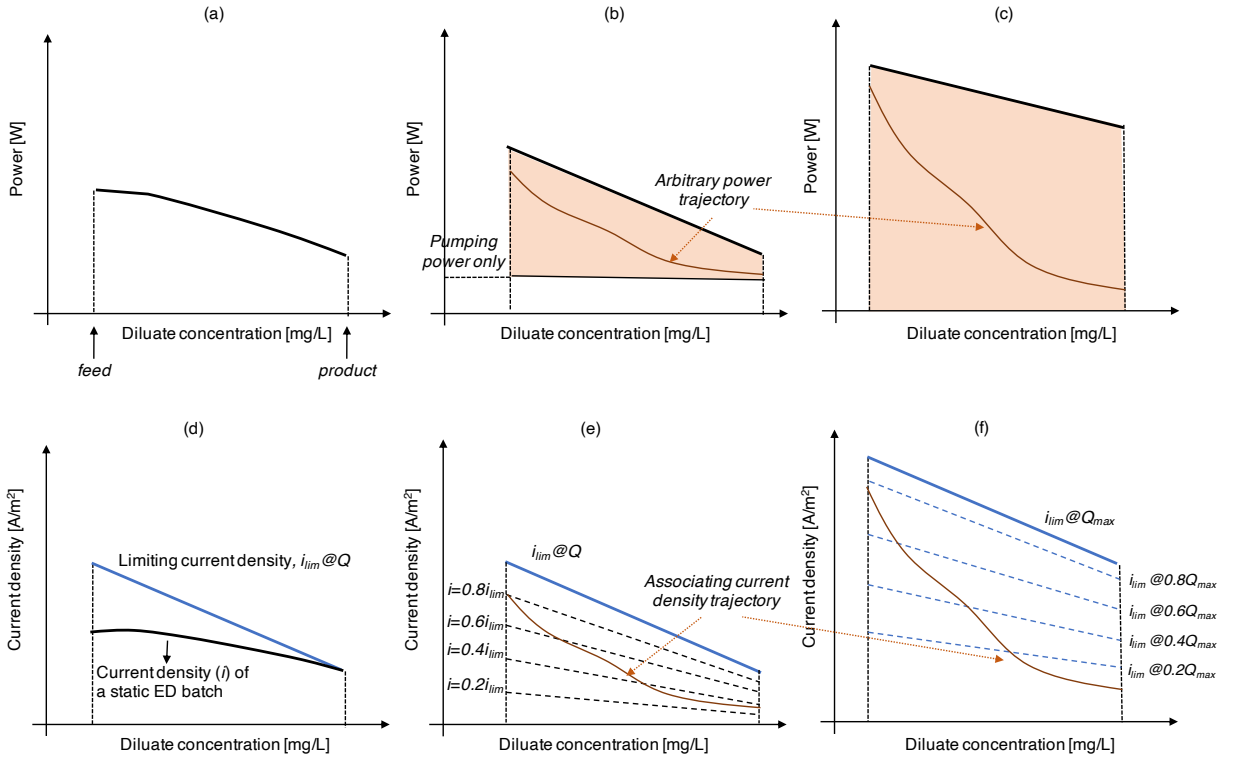

Figure 2: The operational domains of static, voltage-controlled, and voltage- and flow-controlled ED batch operations. (a) The power curve of a conventional static ED batch process (solid line). (b) The flexible power domain of a voltage-controlled ED batch process with constant flow rate (shaded area). (c) The flexible power domain of a voltage- and flow-controlled ED batch process (shaded area). (d) Applied current density and limiting current density of a conventional static ED batch process. The solid black line shows how applied current density changes over a batch as the diluate concentration is reduced. (e) The flexible operational domain of the current density for a voltage-controlled ED batch process with constant flow rate. The dashed lines show ratios of applied current density to limiting current density. (f) The flexible operational domain of the limiting current density for a voltage- and flow-controlled ED batch process. The dashed lines show limiting current densities at varying flow rates. The shaded regions in each plot show the operational domains where a batch ED process could be operated. In b and c, an arbitrary trajectory of a variable power source is shown, with the corresponding applied current density trajectory to produce water shown in e and f, respectively. i_{lim} and i are limiting current density and applied current density, respectively. Q is flow rate. Q_{max} is the flow rate corresponding to maximum power utilization in voltage- and flow-controlled ED operation.

able to operate. Figure 2a depicts a typical power consumption pattern during a static ED batch, in which a constant voltage and a constant flow rate are applied. At each diluate concentration, as the batch desalinates from feed to product, the power consumption is fixed regardless of input power available. Static ED operation does not have any flexibility, requiring the power source (e.g. the grid or a solar system with batteries) to be able to match the fixed desalination power demand. Figure 2d depicts the current density throughout a batch static ED process, which represents the ion transfer rate across the membranes. With higher applied current density the system can desalinate faster. The limiting current density determines a condition where the ion concentration at the interface of the membrane reaches zero, which is the maximum salt removal rate before entering the overlimiting regime in ED systems [28]. If the current density is higher than the limiting current density, other phenomena (e.g. electroconvection and water splitting [32]) will occur to withstand a higher current. This study focuses on conventional ED operations in which the current density is no higher than the limiting current density. ED with overlimiting currents is beyond the scope of this study.

In a conventional static ED batch, the applied voltage is determined by setting the current density below the most constraining limiting current density, which occurs at the end of the batch (Fig. 2d). As a result of this constraint, the applied current density is much lower than limiting at other points in the batch process, resulting in underutilized capacity of the membranes throughout much of the batch, and a salt removal rate that is lower

than the maximum possible.

Voltage-controlled ED creates an additional degree of freedom in control by changing voltage applied to the ED stack to manipulate the applied current density. This functionality can be used to either maximize water production by setting the current density always close to limiting (as proposed by Shah et al. [28]), or to maximize utilization of variable power by actively controlling the current density between zero and limiting. In a voltage-controlled batch ED operation with a constant flow rate, the maximum ED power (associated with the electrical field for removing, details in Section 3) is determined by the ED operation at the highest current density, i.e. limiting current density; the pumping power in a voltage-controlled ED system, as presented by Shah et al., is constant. The flexible power range of this system is illustrated in Fig. 2b. Any power trajectory in the flexible power range (Fig. 2b) can be met by varying the current density during desalination via voltage control (Fig. 2e). Although a voltage-controlled ED system can be operated in a flexible domain, the applied current density may be substantially lower than limiting due to power restrictions imposed by a variable power source (Figs. 2b and e). Therefore, voltage-controlled operation may also underutilize the ED membranes to produce water.

To simultaneously co-maximize water production per unit membrane area and variable power utilization, control over a second degree of freedom – flow rate – is proposed. Adding flow control enables an ED system to actively vary its limiting current density, in addition to varying the applied current density via voltage control. Under this control scheme, the flow controller would optimally set the flow rate to set the appropriate limiting current density to fully utilize available power (as illustrated by the dotted lines in Fig. 2f, details can be found in Section 3). At the same time, the voltage controller would ensure the ED system was operating near the "flow-controlled" limiting current density for fully utilizing the membrane capacity. Therefore, voltage- and flow-controlled ED can always maximize water production rate while fully utilizing a variable power resource. Furthermore, as illustrated in Fig. 2c), the upper boundary of power consumption in voltage- and flow-controlled ED can be much higher than in static ED or voltage-controlled ED for a given system size, as increasing flow rate increases limiting current density and the power threshold. Note in Fig. 2c) that the power domain can be reduced to zero by slowing the pumping flow rate to zero.

3. Model-based controller for voltage- and flow-controlled ED batch operation

This section presents a control strategy in which water production and variable power utilization are co-maximized using two degrees of freedom in the ED system - the voltage and flow rate. Water production rate, which is dependent on desalination rate, is maximized by adjusting the voltage at each time step such that the applied current density is maximized without exceeding the limiting current density. Variable power utilization is maximized by adjusting the flow rate at each time step such that the power consumed closely follows the power available from the source.

In our prior work, a robust ED static-operational model was proposed and validated [33]. This model parametrically describes the mass flow and power transfer between components (e.g., ED stack, pumps, etc.) and was demonstrated on multiple sizes of ED systems. This model is used herein to develop the time-variant ED control theory.

The static ED model is first discretized temporally into multiple controlling time steps, τ_i, each of which can be assigned a varying voltage and flow rate. At each time step, the ED operation starts with a bulk diluate concentration, $C_{d,0}^{b,\tau_i}$, and a bulk concentrate concentration, $C_{c,0}^{b,\tau_i}$, at the point between each respective tank and the ED stack inlets (illustrated in Fig. 3a). When a voltage is applied, a concentration boundary layer of thickness δ within a flow channel in the ED stack extends from the membrane surfaces, where the concentration is $C_{d/c,y}^{AEM/CEM,\tau_i}$, to the bulk flow, where the concentration is $C_{d/c,y}^{b,\tau_i}$. The scripts b, AEM, CEM, d, and c designate bulk flow, the boundary layers near the AEM or CEM membrane, and the diluate or concentrate streams, respectively. The subscript y denotes the location along the discretized flow path, with Y the total discretized flow segments.

The ion increase/removal rate of concentrate/diluate is controlled by varying the voltage, V^{τ_i}, and the flow rates of the concentrate and diluate streams, $Q_c^{\tau_i}$ and $Q_d^{\tau_i}$, respectively:

$$\begin{aligned}(\frac{dC_{d,y}^{b}}{dt})^{\tau_i} =& \frac{1}{NV_y^{cell}}[Q_d^{\tau_i}(C_{d,y-1}^{b} - C_{d,y}^{b})^{\tau_i} - \frac{N\phi I_y^{\tau_i}}{zF} \\ &+ \frac{NA_yD^{AEM}(C_{c,y}^{AEM} - C_{d,y}^{AEM})^{\tau_i}}{l^{AEM}} \\ &+ \frac{NA_yD^{CEM}(C_{c,y}^{CEM} - C_{d,y}^{CEM})^{\tau_i}}{l^{CEM}}], \text{ and}\end{aligned} \tag{1}$$

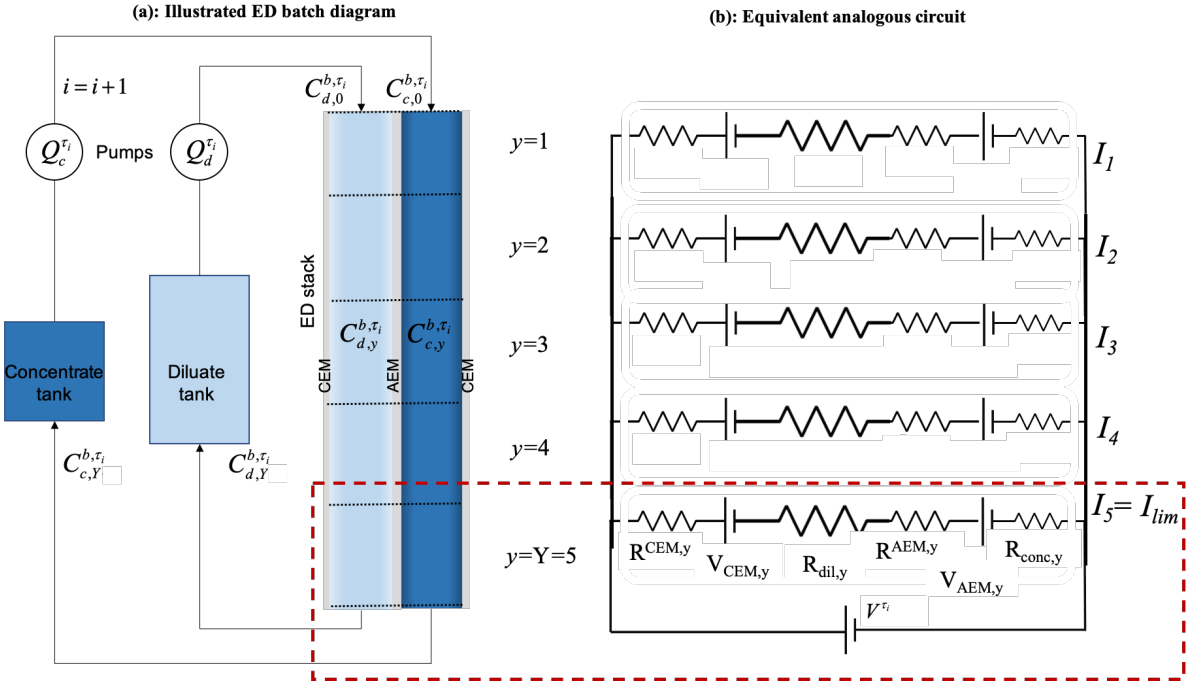

Figure 3: The illustrated flow of the diluate and the concentrate streams in an ED batch system with the associated electrical circuit model used to simulate time-variant ED operation. (a) The two streams in a batch ED system. For every control time step (τ_i), $Q_d^{\tau_i}$, $Q_c^{\tau_i}$, and V^{τ_i} represent the flow rate for the diluate, concentrate, and the voltage, respectively. The simulation model is described starting from the inlet of the stack to the outlet of the tanks, where the time step is updated ($i = i + 1$). C_d and C_c denote the concentration of the diluate and the concentrate, respectively. $y = 1, 2, ..., Y, Y + 1$ denote segment locations along the flow path. (b) The equivalent electrical circuit for the ED stack. The dashed line represents one segment (one value of y) and its equivalent circuit model. $R^{AEM,y}$ and $R^{CEM,y}$ are the area resistances associated with the AEM and CEM membranes, respectively. $V_{AEM,y}$ and $V_{CEM,y}$ are the potentials across the AEM membrane and the CEM membranes, respectively. $R_{d,y}$ and $R_{c,y}$ are the area resistances associated with the AEM and CEM membranes, respectively. I is the current flowing through the ED stack. I_{lim} is the current when the applied current density equals to the limiting current density.

$$\begin{aligned}(\frac{dC_{c,y}^b}{dt})^{\tau_i} =& \frac{1}{NV_y^{cell}}[Q_c^{\tau_i}(C_{c,y-1}^b - C_{c,y}^b)^{\tau_i} + \frac{N\phi I_y^{\tau_i}}{zF} \\ &- \frac{NA_y D^{AEM}(C_{c,y}^{AEM} - C_{d,y}^{AEM})^{\tau_i}}{l^{AEM}} \\ &- \frac{NA_y D^{CEM}(C_{c,y}^{CEM} - C_{d,y}^{CEM})^{\tau_i}}{l^{CEM}}],\end{aligned} \tag{2}$$

where V_y^{cell} is the volume of each segment, z is the ion charge, F is Faraday's constant (96,485 C/mol), N is the number of cell pairs, I is the current, A is the membrane area, $D^{AEM/CEM}$ is the diffusion coefficient in the AEM and CEM membranes, respectively, and l is the thickness of membranes. ϕ is the current leakage factor, also called current efficiency, which accounts for the loss of current that occurs when an electrical path parallel to the active channel area exists for the current to flow through. Current leakage can be assumed negligible for a well-designed stack [33].

The diluate and the concentrate streams flow out from the ED stack and mix with the water in the diluate and concentrate tanks, respectively. The rate of concentration change in the diluate and concentrate tanks can be described as

$$(\frac{dC_{d,0}^b}{dt})^{\tau_i} = \frac{Q_d^{\tau_i}}{V_d^{tank}}(C_{d,Y}^{b,\tau_i} - C_{d,0}^{b,\tau_i}), \text{ and} \tag{3}$$

$$(\frac{dC_{c,0}^b}{dt})^{\tau_i} = \frac{Q_c^{\tau_i}}{V_c^{tank}}(C_{c,Y}^{b,\tau_i} - C_{c,0}^{b,\tau_i}), \tag{4}$$

where $C_{d,0}^b$ and $C_{c,0}^b$ are the concentrations of the diluate and concentrate tanks (and ED stack inlets), respectively, and V_d^{tank} and V_c^{tank} are the volumes of the diluate and concentrate tanks, respectively. The desalination rate of the ED system is the desalination rate of the diluate tank, given by Eq. 3.

To calculate the total current, the ED stack is modeled as an analogous DC circuit (Fig. 3b), with a current flowing through each discretized segment

$$I_y^{\tau_i} = \phi_A(\frac{WL}{Y})i_y^{\tau_i}, \tag{5}$$

where W is the stack width, L is the membrane channel length, ϕ_A is the open area porosity of the turbulence-promoting channel spacer, and i is the current density. The equivalent circuit elements for each discretized segment are connected in parallel, and thus the voltage is equal across all segments.

To maximize the desalination rate at a given flow rate, the segment current should be maximized, as indicated by Eq. 1. The limiting current density determines the maximum applied current density that can be supported by the ED system before overlimiting phenomena occurs, as discussed in Section 2. It can be approximated as a function of the bulk diluate concentration with

$$i_{lim,y}^{+,-} = \frac{zFkC_{d,y}^b}{t^{AEM,CEM} - t^{+,-}}, \tag{6}$$

where $t^{+,-}$ is the minimum of the dimensionless anion (-) and cation (+) transport numbers in the bulk solution. $t^{AEM,CEM}$ are the transport numbers of the AEM and CEM membranes, respectively, which are assumed to be 1 in this study. In the bulk solution, for a single 1-1 electrolyte such as NaCl, the limiting current density is determined by the lower of the two solution transport numbers. k is the mass transfer coefficient. k can be represented as

$$k = \frac{ShD_{aq}}{d_h}, \tag{7}$$

where D_{aq} is the diffusion coefficient of the aqueous solution, d_h is the hydraulic diameter, and Sh is the Sherwood Number. Sh represents the mass transfer performance, and is correlated with the Reynolds number and the Schmidt number. These relationships are described further in Appendix A.

As indicated by Eq. 6, the limiting current density is proportional to the bulk diluate concentration. As the voltage increases, the applied current density of the last segment ($y = Y = 5$) is the first to reach the limiting current density because the bulk diluate concentration at the outlet is the lowest within the ED stack. Thus, the maximum voltage that can be applied without exceeding the limiting current density is the voltage when the applied current density of the last segment is close to the limiting current density. This maximum voltage is

$$\begin{aligned} V^{\tau_i} =& V_{el} + N(V_Y^{CEM} + V_Y^{AEM}) + Nr_i i_{lim,Y}(R_{d,Y} \\ &+ R_{c,Y} + R_Y^{BL} + R^{AEM,Y} + R^{CEM,Y}), \end{aligned} \tag{8}$$

where: V_{el} is the electrode potential (1.4 V when hydrogen ions are reduced at the cathode and hydroxide ions are oxidized at the anode); $V_{CEM,Y}$, $V_{AEM,Y}$ are the potentials across the CEM and AEM membranes, respectively; R_Y^{BL}, $R^{AEM,Y}$, $R^{CEM,Y}$ are the area resistances associated with the concentration boundary layers, the AEM membranes, and CEM membranes, respectively; and r_i is the safety factor for approaching the limiting current density. r_i provides an additional degree of freedom to track (with an appropriate safety-margin) the limiting current density throughout the batch process [31]. $R_{d,Y}$ and $R_{c,Y}$ are the resistances associated with the diluate and concentrate streams, respectively, which can be further represented as

$$R_{d,Y} = R_{d,Y}^b + R_{d,Y}^{AEM} + R_{d,Y}^{CEM}, \text{and} \tag{9}$$

$$R_{c,Y} = R_{c,Y}^b + R_{c,Y}^{AEM} + R_{c,Y}^{CEM}, \tag{10}$$

where $R_{d/c,Y}^b$ is the resistance of the bulk flow, and $R_{d/c,Y}^{AEM}$ and $R_{d/c,Y}^{CEM}$ are the resistances in the boundary layers near the membrane surfaces, respectively. These equivalent resistances depend on the diluate and concentrate concentrations; detailed derivations for these resistances can be found in Wright et al. [33].

The potentials associated with the concentration difference across the exchange membranes, $V_{AEM,Y}$ and $V_{CEM,Y}$, can be approximated by

$$V_{AEM,Y} = \frac{(2t^{AEM} - 1)RT}{F} \log(\frac{\gamma_c C_{c,Y}^{AEM}}{\gamma_d C_{d,Y}^{AEM}}), \text{and} \tag{11}$$

$$V_{CEM,Y} = \frac{(2t^{CEM} - 1)RT}{F} \log(\frac{\gamma_c C_{c,Y}^{CEM}}{\gamma_d C_{d,Y}^{CEM}}), \tag{12}$$

where T is the temperature and R is the gas constant, $8.31 JK^{-1}mol^{-1}$ [33].

To maximize variable power utilization, total system power consumption is adjusted to closely follow the input power. The total system power consumption of a time-variant ED system is estimated by summing the power consumption of the most power-consuming components, which are the DC power supply for the ED stack and the diluate and concentrate pumps:

$$P_{total}^{\tau_i} = P_{ED}^{\tau_i} + P_{pump,d}^{\tau_i} + P_{pump,c}^{\tau_i}, \tag{13}$$

where $P_{pump,d}$ and $P_{pump,c}$ denote the power consumed by the diluate pump, and the concentrate pump, respectively. P_{ED} denotes product of the voltage and current applied to the ED stack.

The power consumed by the variable speed pumps of the diluate and concentrate streams will depend on the flow rate and the hydraulic characteristics of the full ED system. In general, the power consumption of a variable speed-controlled centrifugal pump follows the Affinity Laws (also known as "the Pump Laws") [34],

$$\frac{Q_{d/c}^{\tau_i}}{Q_{ref}} = \frac{n_{d/c}^{\tau_i}}{n_{ref}}, \tag{14}$$

$$\frac{H_{d/c}^{\tau_i}}{H_{ref}} = (\frac{n_{d/c}^{\tau_i}}{n_{ref}})^2, \text{and} \tag{15}$$

$$\frac{P_{pump,d/c}^{\tau_i}}{P_{ref}} = (\frac{n_{d/c}^{\tau_i}}{n_{ref}})^3, \tag{16}$$

where n is pump speed and H is the pump head. Q_{ref}, H_{ref}, P_{ref}, and n_{ref} indicate the referenced operation points of the system.

The power consumption of the DC power supply in an ED stack (i.e. the desalinating power) is estimated as the product of the current and the applied voltage,

$$P_{ED}^{\tau_i} = (VI)^{\tau_i}. \tag{17}$$

To match the instantaneous power input, the instantaneous power consumption of the ED system, $P_{total}^{\tau_i}$, is controlled by varying the voltage and flow rate. As shown by Eq. 14 and Eq. 16, the pumping power explicitly depends on the flow rate, which can be used to estimate the new pumping power when a new flow rate is applied.

To estimate the new desalinating power, $P_{ED}^{\tau_i}$, when a new voltage is applied to the ED stack is non-trivial. It requires summing all of the segments' currents, as shown in Fig. 3, which requires solving a system of equations, including Eq. 1 and Eq. 2, at varying flow rates. However, variable power inputs from solar or wind sources, or changes in electricity tariffs in dynamic grid pricing, may vary on the order of seconds, requiring the controller to respond quickly to identify and apply optimal voltages and flow rates. To accelerate the controller's computational efficiency, an explicit method of estimating the ED desalination power under varying flow rate conditions is proposed.

To reduce computation time, the controller only considers electromigration for ion transfer. Electromigration generally contributes ≥90% of the mass transfer in ED desalination [33, 35], and the contribution is even higher with a high current (enabled by a high flow rate, as indicated by Eq. 6). This assumption results in the explicit current estimation

$$I_{appr}^{\tau_i} = \frac{Q_d^{\tau_i}(C_{d,0}^b - C_{d,Y}^b)^{\tau_i} zF}{N\phi}, \tag{18}$$

where $I_{appr}^{\tau_i}$ is the approximated current. In this case, the transience of the changing flow rate is negligible compared to the transience of the changing dilute concentration, due to the incompressible nature of water.

Using the approximated current (Eq. 18) and the maximized voltage (Eq. 8), the ED desalination power at the new flow rate can be explicitly estimated (Eq. 17). The total power consumption can then be evaluated at a different flow rate and combined with Eq. 16, which enables the controller to efficiently optimize flow rates to match or closely follow the available variable power input.

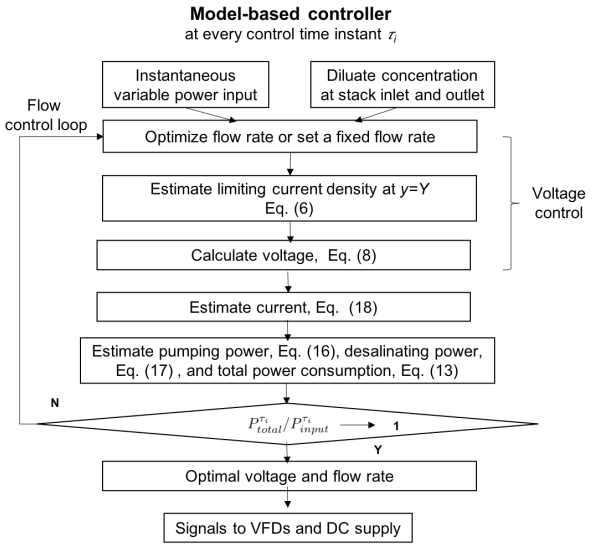

Figure 4: Flowchart of the model-based controller for time-variant ED operation. $P_{total}^{\tau_i}$ and $P_{input}^{\tau_i}$ are the total power consumption (including the ED power and the pumping power) and the variable power input at every control time instant τ_i, respectively. Y refers to the total discretized sections of the ED stack referenced in Fig. 3.

Figure 4 shows a flowchart of the final model-based controller, incorporating both desalination rate and power utilization components. By using this controller, water production is maximized by setting a voltage that maximizes the ion transfer rates and avoids water splitting occurring in the stack at a particular flow rate. Then the variable power utilization is maximized by setting the flow rate using an optimization feedback loop that minimizes the difference between the power consumption

and the available power input. As a result, this strategy enables the simultaneous maximization of water production and variable power utilization, facilitating the most efficient use of water and available power at every point in time.

4. Pilot time-variant ED system design

4.1. Experimental setup

A pilot-scale time-variant ED prototype was built to validate the proposed control theory, following the configuration shown in Fig. 5. The ED stack (model AQ3-1-2-50-35), the CEM membranes (model CR67HMR) and the AEM membranes (model AR204SZRA) were manufactured by Suez Water Technologies and Solutions [36]. Parameters of the ED stack and membranes are listed in Table 1, in which other parameters used in the analysis of the ED system are also included. Detailed justification of the parameters used in this study can be found in [33]. Two pumps (Xylem Goulds 3SV-11) recirculated the diluate and concentration streams with their speed controlled by pump controllers (Xylem CentriPro Aquavar). A 60-25V DC supply (TDK-Lambda GEN) supplied the voltage (regulated to ±1% of the commanded value). The electrical polarity of the applied voltage was reversed between batches; during reversal, the diluate and concentrate channels in the stack were switched using valves. This reversal operation has been shown to reduce the scaling propensity in ED desalination [37]. No significant scaling occurred during the testing in this study.

Two flow meters (Omega FP1408) were used to monitor the flow rate (±1%) in the diluate and concentrate streams. In-line conductivity probes (Connectivity Instruments CDCE-90) interfacing with conductivity controllers (Connectivity Instruments CDCN-91) monitored the conductivity (to an accuracy of ±2%) at the entry and exit of the ED stack. All sensors interfaced with a CLICK I/O Programmable Logic Controller (PLC) with analog input and output modules (C0-04AD-1, C0-04AD-2, and C0-04DA-2). Each electrode was rinsed with a sodium sulfate solution (conductivity over 14 mS/cm ±2%) held at a flow rate of 6-8 LPM (±1%).

Feed water was taken from Well No. 1 at the Brackish Groundwater National Desalination Research Facility (BGNDRF) in Alamogordo, New Mexico. Major constituents in the water are listed in Table 2. The feed water salinity was similar to that of a previous pilot-scale PV-ED field study conducted by our group in rural India [12]. Water quality measurements were performed by DHL Laboratories (San Antonio, TX). In each batch reported in the following section, the feed water was desalinated to a target product concentration of 500 μS/cm with a batch size of 0.42 m^3.

Variables	**Value**
Parameters of the ED stack	
ED cell pairs	30
Diluate tank volume, m^3	0.42 ±4%
Brine tank volume, m^3	0.28 ±7%
Flow Path Width, cm	19.7
Flow Path Length, cm	168
AEM Resistance, $\Omega\,$cm^2	7
CEM Resistance, $\Omega\,$cm^2	10
Void fraction	0.83±0.03
Area porosity	0.70±0.02
Spacer thickness, mm	0.71±0.01
Other parameters	
F, C mol^{-1}	96,485
D^{AEM}, m^2 s^{-1}	3.28×10^{-11}
D^{CEM}, m^2 s^{-1}	3.28×10^{-11}
D_{aq}, m^2 s^{-1}	1.6×10^{-9}
t^+	0.39
t^-	0.61
z	1
ϕ	1

Table 1: Parameters of the ED stack

Parameters	**Value**
Na^+, mg L^{-1}	293±29
Mg^{2+}, mg L^{-1}	12.6±1.3
Ca^{2+}, mg L^{-1}	54.6±5.5
Cl^-, mg L^{-1}	38.1±3.8
SO_4^{2-}, mg L^{-1}	504±50
Alkalinity Bicarbonate, mg L^{-1} as $CaCO_3$	161±1
Total dissolved solids (TDS), mg L^{-1}	995±72
Conductivity, μS cm^{-1}	1,500±30

Table 2: The major constituents in the brackish groundwater from Well NO.1 at the Brackish Groundwater National Desalination Research Facility (BGNDRF), measured on 3-Dec-2018.

4.2. Controller implementation

The pump speeds and voltage applied to the ED stack electrodes were controlled by variable frequency drives (VFDs) and a programmable DC power supply according to the received control signals from the implemented

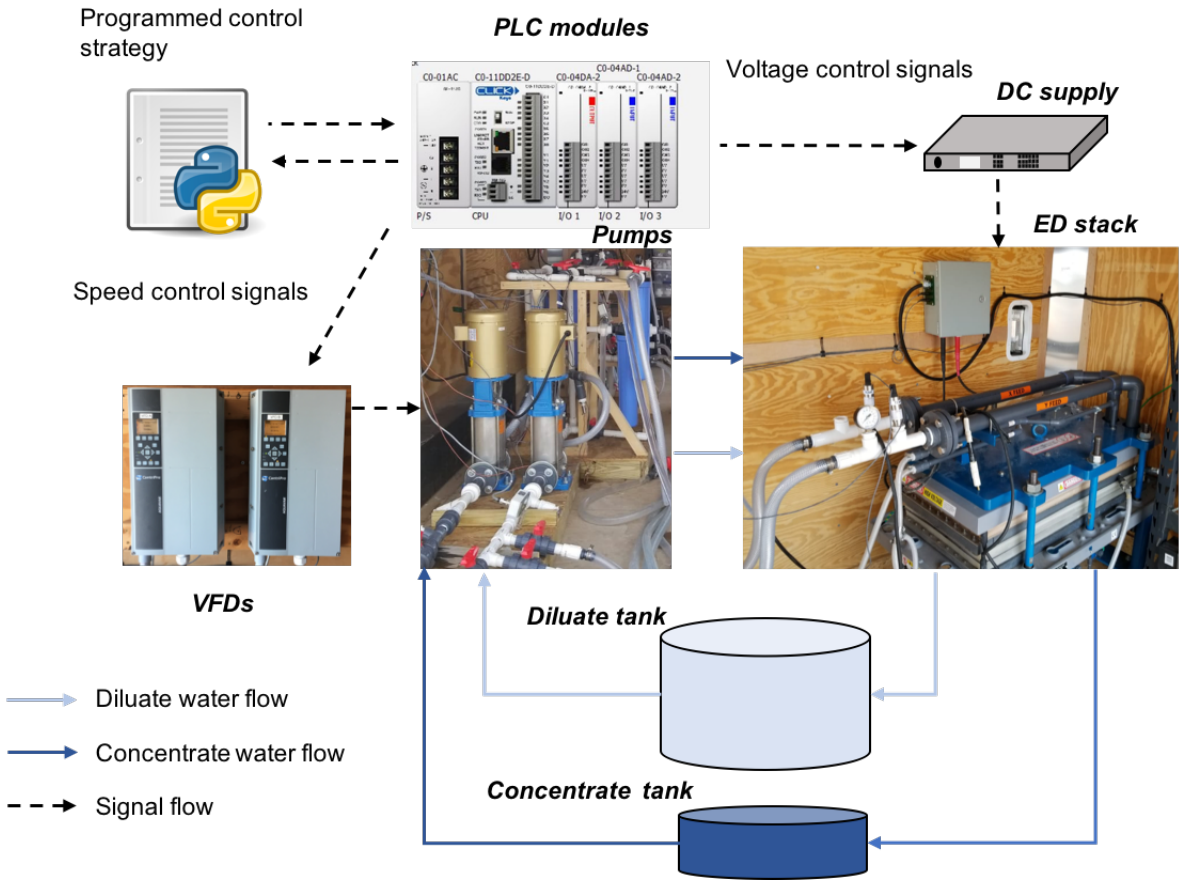

Figure 5: Major system elements and their interactions for the time-variant ED prototype tested at the Brackish Groundwater National Desalination Research Facility (BGNDRF) in Alamogordo, New Mexico.

controller script, respectively. The controller strategy, implemented in Python, calculated an optimal voltage and flow rate using real-time measurements of variable power inputs and conductivity from both the diluate and concentrate streams, based on the model introduced in Section 3. Pump performance curves were experimentally generated from the two installed pumps based on measurements at multiple speeds. Speed versus flow and speed versus power pump curves were empirically fit to the experimental data and used in the controller implementation, as described in Section 3. The fitted pump curves are plotted in Appendix B.

Control signals were applied to the time-variant ED prototype in an open loop. Communication between the controller script and modules in the prototype was implemented via PLC modules. Using measured concentrations at the current time, controller predictions were used to optimize the flow rate and voltage. Signals for these values were then sent to the VFDs and the DC power supply to control the flow rate and voltage, respectively, for the upcoming time step. The duration of the time step was 3 s, based on preliminary testing and chosen to capture variations in the power input while allowing enough time for the ED system to reach a new steady state after the latest change in voltage and flow rate. The system response time was determined experimentally. The same time step of 3 s was used for simulation studies.

5. Pilot time-variant ED system testing and results

5.1. Controller test for variable voltage, high constant flow rate ED

The efficacy of the control theory presented in Section 3 was first tested with a fixed, high flow rate and variable voltage to see if the controller could produce an increased desalination rate compared to static ED operation. The maximum flow rate in an ED system

depends on many factors and is determined by the maximum pump speed. In this study, the maximum linear velocity in the membrane channels was restricted to be ~20 cm/s (±1%), corresponding to 42 LPM bulk flow rate. This is already significantly higher than the velocity in the membrane channels of conventional static ED operation (4-12 cm/s) [28], which is set to ensure operational stability of the membranes and spacers. Figure 6 shows the current density, power consumption, and diluate conductivity over a batch for voltage-controlled ED operation at the maximum flow rate of 42 LPM. Static ED operation with a flow rate of 25 LPM (~12 cm/s in the membrane channels) is shown for comparison. In these tests, the current density was not allowed to exceed 70% of limiting (which is a function of flow rate, described in Section 3).

Figure 6 demonstrates that running the time-variant ED prototype at a high flow rate increased the operational domain (shaded region) compared to the single operating trajectory for static ED (black line), achieving a 45% increase in desalination rate (Fig. 6c). Further comparisons of static ED to time-variant ED at different flow rates are shown in Appendix C. The controller predictions and the experimentally measured current and power were consistently aligned (within 1.5% RMS error). This indicates that the controller can accurately predict current and then successfully predict power consumption. The results in Fig. 6 show that the controller could enable the time-variant ED system to directly use variable power sources over a wide range of operating conditions by varying flow rate and ED stack voltage, as discussed in Section 3.

5.2. Controller test for voltage- and flow-controlled ED

To further characterize the performance of voltage- and flow-controlled ED operation, and validate the control theory presented in Section 3, the time-variant ED prototype system was run using a representative solar power input profile (Fig. 7a) during one batch. The solar profile was recorded by a set of local solar panels (Hyundai HiS-S285RG) at BGNDRF. The target product concentration was set to 300 mgL^{-}1 (~500 μS cm^{-1}) for this test. The controller was able to command the prototype ED system to consumer power on a trajectory that closely followed (within 10.0% RMS error) the reference solar power profile (Fig. 7a) while maintaining a measured product water concentration of 300 mgL^{-}1. These results demonstrate the ability of the time-variant ED system to adaptively desalinate water to a desired product concentration while adjusting voltage and flow rate to match an arbitrary variable power level. This flexibility could allow the time-variant ED system to directly integrate with real clean energy sources, such as solar or wind, without requiring significant battery capacity.

Figure 7b shows the controlled power consumption profile of the pilot-scale time-variant ED system while the controller was fed three arbitrary constant input power levels of 1000 W, 850 W, and 730 W. Constant power levels were chosen as inputs for three primary reasons. First, any variable power source can be approximated as constant for a very short duration. Second, at each controlling time step (every 3 s in these experiments), the controller needs to optimize and adjust voltage and flow rate to match a singular power value; whether this value changes in time or not is arbitrary in the perspective of the controller. To maintain a constant power consumption, the controller has to continuously make adjustments, just as it would to follow a variable input power profile. Third, operating a constant power while maximizing water production rate simulates real-world situations where power consumption would have to be maintained under a threshold, say within the speed limitations of a wind turbine or in an industrial grid-powered application where there are different charge rates depending on power draw. Therefore, the three constant power levels were used to robustly test the load flexibility of the prototype time-variant ED system and demonstrate the utility of the control model.

The results in Fig. 7b demonstrate that the controlled time-variant ED system power consumption was able to closely match the predefined constant input power levels for all three cases; the RMS errors for each test were 1.7% for 1000 W, 4.2% for 850 W, and 6.3% for 730 W, as the batch desalinates from 1400 μS/cm to about 500 μS/cm. All of the time-variant ED operations had higher desalination rates (ranging from 6-15%) than the static ED process used as a benchmark (Fig. 7c). The shaded regions in Figs. 7a and b show how much flexibility remains in the operational domain, with the upper limit bounded by the same maximum power conditions shown in Fig. 6, defined by variable voltage operation and a constant pumping flow rate of 42 LPM.

5.3. Desalinating and pumping power

Although the time-variant ED batch trajectories largely align with their respective input power profile, there are some small deviations. Particularly in the cases with relatively low power input, the measured experimental power tends to fluctuate around the variable power input. To explore this deeper, the data from Fig. 7b were decomposed to analyze the power contributions from the ED desalination process and pumping.

Figure 8 shows that the measured and predicted ED desalination power values follow the same trends for the

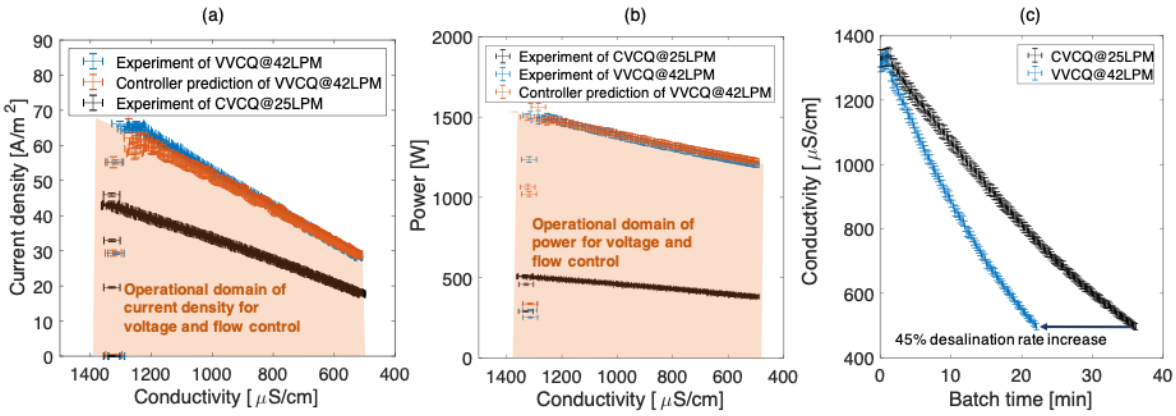

Figure 6: Controller predictions and experimental ED batch performance under voltage-controlled variable voltage (VV) and high constant flow rate (CQ) (42 LPM) conditions versus constant voltage (CV), moderate constant flow rate (CQ) (25 LPM) conditions. Results are presented for: (a) current density versus diluate conductivity; (b) total power of the ED system versus diluate conductivity; and (c) diluate conductivity versus batch time (experimental performance only). The shaded regions in (a) and (b) represent the flexible operational domain for which a flexible ED system could operate using direct power from a variable power source.

three tested cases. However, for power levels of 850 W and 730 W, the measured total desalination power is slightly under the predicted power. These deviations are likely due to the neglected back diffusion through the membranes into the channels; because the controller does not take back diffusion into account, it tends to predict a higher current for a given applied voltage (Eq. 18). The power becomes increasingly over-predicted at lower flow rates because the back diffusion is higher, as seen in the 850W and 730W cases.

The measured pumping power follows the general trend of the predicted pumping power in all of the tested cases, with the exception of some small fluctuations in the 850 W and 730 W cases (Figs. 8b and c, respectively). The small fluctuations at lower input power levels may be caused by the behavior of the pump when operating outside its intended performance curve. The applied voltage and flow rate in the three cases are plotted in Figs. 9a and b, respectively. The pumps used in the prototype ED pilot have their highest efficiency at flow rates of 40-70 LPM. Figure 9b plots the flow rate for each input power level during the ED batch. The pumps were operated in a region outside their intended performance curve for the lower power levels of 850 W and 730 W, where they would be expected to perform less predictably and stably. They were operated closer to their high efficiency operation zone at the power level of 1,000 W. A slightly downsized pump may have improved the power fluctuations seen in Fig. 8. In spite of these small fluctuations, the measured pumping power closely followed the values predicted by the controller (to within 1.8% RMS for 1000 W, 4.6% RMS for 850 W, and 5.7% RMS for 730 W, as the batch desalinates from 1400 μS/cm to about 500 μS/cm).

A large spike in the voltage is apparent in Fig. 9a at the beginning of each batch for all three power levels, accompanied by a rapid drop in flow rate just before the voltage spike. These features are caused by an underprediction of current at the beginning of the batch by the controller. At this moment, the electric potential is instantaneously applied across the membranes in the ED stack. In a real stack, for the initial diluate concentration in the membrane channels to be perturbed by the electrical field, salts must accumulate before building up concentration variations between the inlet and outlet. These transient effects are ignored by the controller, and therefore, the approximated current from Eq. 18 underestimates the applied current at this moment, causing an overprediction of flow rate in the first few instants, as seen in Fig. 9b. After the voltage spike, the concentration drop across the diluate stream becomes fully developed and the effect of the accumulating salts becomes insignificant. During this transient period, the control model has a large error (compared to the period after the spike) due to the assumptions used in the model being briefly invalid. Therefore, for this short duration, a small amount of battery energy storage is required to supply enough power. This transient period is generally very short (less than 1 min per 25-40 min batch in the pilot system), and the required battery capacity is nearly

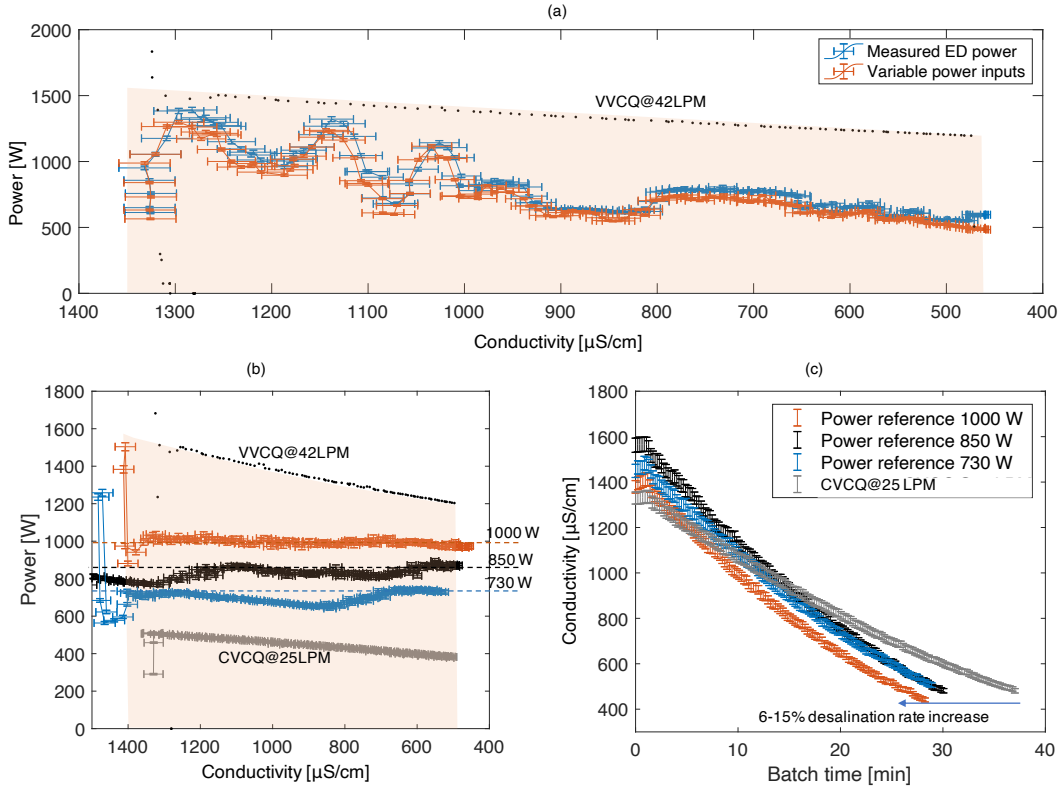

Figure 7: Time-variant ED system performance for varying power inputs. (a) Measured power usage for time-variant voltage- and flow-controlled ED operation from the pilot-scale ED prototype while following a representative, measured solar power profile during one batch. (b) Measured power consumption for time-variant voltage- and flow-controlled ED operation from the pilot-scale ED prototype under three constant power inputs (1000 W, 850 W, and 730 W) during one batch. (c) The corresponding conductivity profiles from the results in (b). A benchmark constant voltage, constant flow rate static ED batch (CVCQ) process at 25 LPM flow rate is shown for comparison in (b) and (c). To demonstrate the operational limits at maximum pumping power, a variable voltage, constant flow rate ED batch process (VVCQ) at 42 LPM is shown in (a) and (b), which marks the upper boundary of the operational domain (shaded region).

negligible. For example, for the pilot time-variant system presented herein that requires batteries for reshaping power over ~1 min, the required battery capacity could be as small as 1/40-1/25 the required battery capacity of traditional renewable-powered ED systems that use batteries to reshape the variable power input throughout the batch.

5.4. The trade-off between production rate and energy consumption

Although voltage and flow rate follow the same trends in variation across the three input power levels shown in Fig. 9, they differ in magnitude. Higher power levels tend to have higher flow rates and higher voltages. Comparing pumping power consumption in Fig. 8 with ED stack voltage in Fig. 9a, the pumping power varies significantly with varying voltage in each of the three power levels, but the measured ED desalination power does not. This indicates that the scaling factors for flow-to-power and voltage/current-to-power differ. Because the feed concentration (~1500 μS cm^{-1}) in each case is desalinated to a same product concentration (~500 μS cm^{-1}), the electrical resistances (Eqs. 9 and 10) of both the concentrate and the diluate streams should be similar, independent of case. As a result, the ED desalination power primarily scales with V^2, according to Eq. 17. In contrast, the pumping power scales with Q^3, according to Eq. 16. As a result, the pumping power increases much faster with flow rate, causing the pumping to consume more power than ED in all three test cases. Efficient pumping is therefore critical to improve the energy efficiency of time-variant ED batch operation.

Table 3 gives the specific energy consumption (SEC) and desalination rate for the three time-variant, voltage- and flow-controlled ED batch cases at different power inputs, along with a static ED batch process with a flow rate

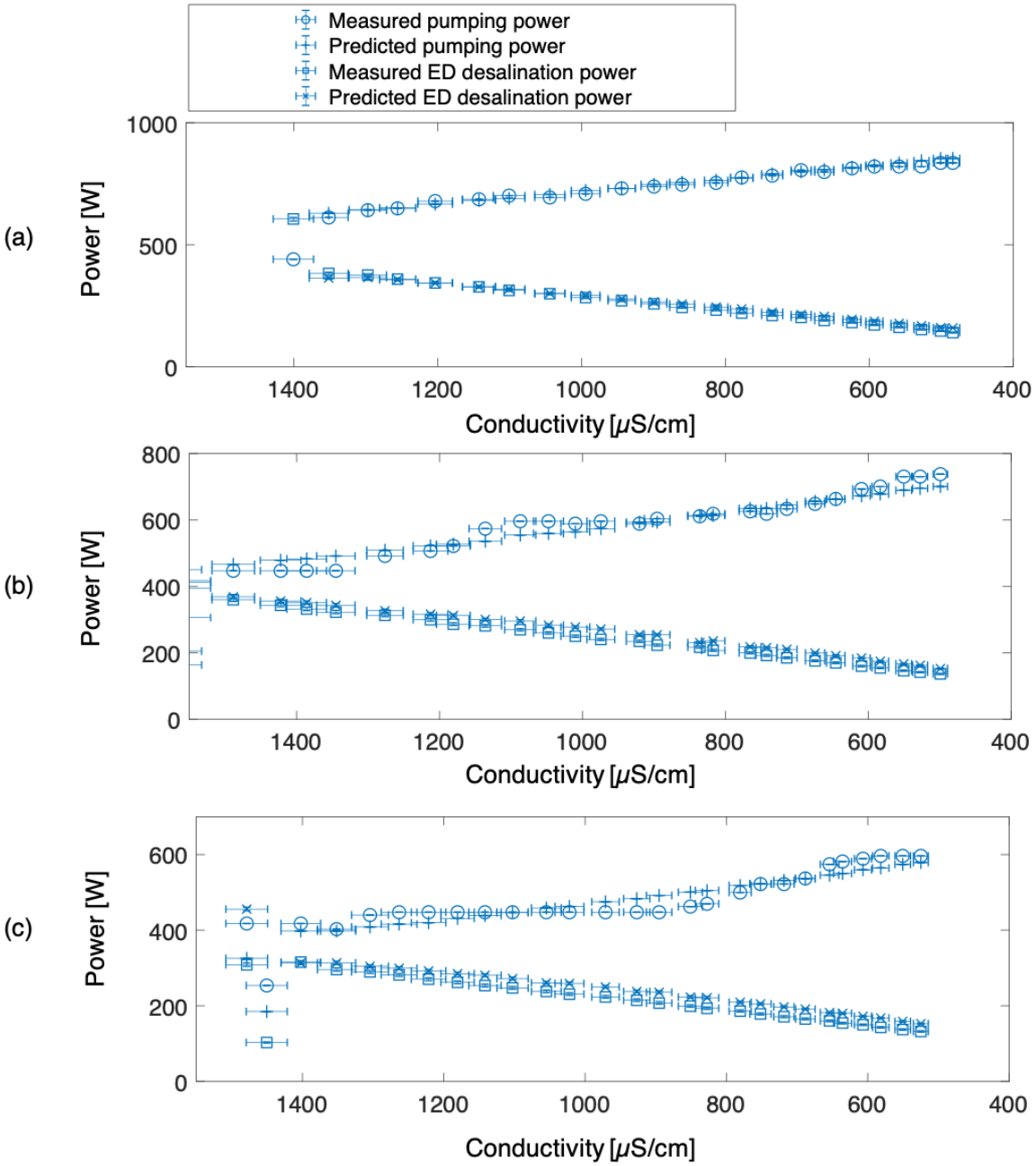

Figure 8: Experimentally measured power consumption of the pump and the ED desalination process, and the controller predictions for reference power inputs of (a) 1000 W, (b) 850 W, and (c) 730 W.

25 LPM. The starting feed concentration was slightly different from batch-to-batch during the experiments; each was run with a target product concentration of 500±5 μS cm^{-1}. The results in Table 3 indicate the trade-off between SEC and batch time (equivalent to desalination rate in m^3/h) and suggest they are correlated non-linearly. The desalination rate was increased by 29%, 20% and 19% by using 62%, 52% and 30% more energy, respectively, compared to static ED. The pumping SEC also corroborates the significantly increased fraction of energy consumed by pumping compared to ED desalination under higher input powers. The percentage

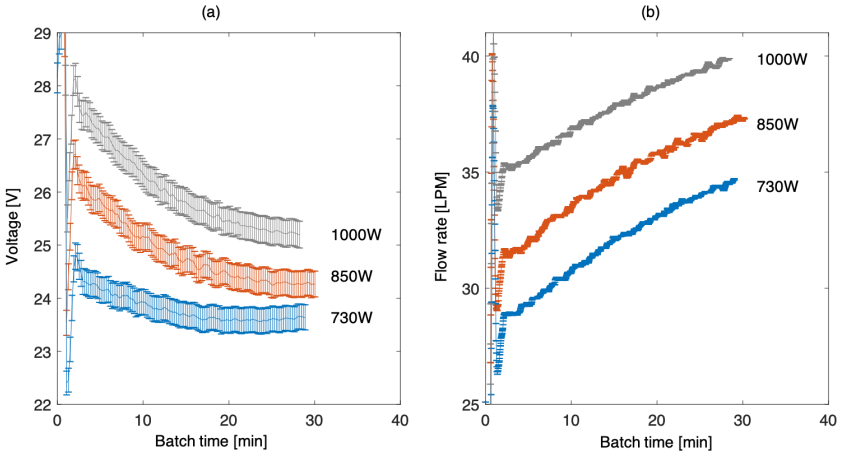

Figure 9: Experimentally measured voltage and flow rates during time-variant ED operation with reference power inputs of (a) 1000 W, (b) 850 W, and (c) 730 W.

Parameters	CVCQ@25LPM	VVVQ@730W	VVVQ@850W	VVVQ@1000W
Feed concentration $[\mu S/cm]$	1340±27	1460±29	1560±31	1410±28
Product concentration $[\mu S/cm]$	500±10	505±10	500±10	500±10
Batch time [min]	35.9±3.3‰	29.0±3.3‰	28.9±3.3‰	25.5±3.3‰
SEC $[kWh/m^3]$	0.63±0.03	0.82±0.04	0.96±0.05	1.02±0.05
Pumping SEC $[kWh/m^3]$	0.43±0.02	0.56±0.03	0.68±0.04	0.75±0.04
ED desalination SEC $[kWh/m^3]$	0.20±0.01	0.26±0.01	0.28±0.01	0.27±0.01
Batch time compared to CVCQ	N/A	82%±5.8‰	81%±5.8‰	71%±5.8‰
SEC compared to CVCQ	N/A	130%±6.8%	150%±7.0%	160%±6.8%
Pumping SEC compared to CVCQ	N/A	130%±7.1%	160%±7.5%	170%±7.1%
ED desalination SEC compared to CVCQ	N/A	130.00%±6.3%	140.00%±6.1%	130.00%±6.2%

Table 3: Performance of the pilot-scale prototype in variable voltage, variable flow (VVVQ), time-variant ED batch operation with constant power inputs of 730W, 850W, and 1000W. Performance of a benchmark constant voltage, constant flow (CVCQ), static ED batch process at a flow rate of 25LPM is given for comparison. All tests were run with a target product concentration of 500±5 μS cm^{-1}.

contribution of pumping to SEC increases from 68% in the static ED case to 74% in the time-variant ED case with input power of 1,000 W.

6. Discussion

In this work, the time-variant method for operating a batch ED system has been demonstrated to be load-flexible and able to accommodate variable power sources and maximize the rate of water production, in order to reduce the water cost. This new operational strategy is analogous to how multi-stage ED stacks, or series assemblies of ED stacks, are arranged with different voltages applied to each electrical stage to maintain applied current density near limiting, and different numbers of parallel flow channels to manipulate flow velocity for a desired limiting current density and/or to minimize pumping power [38]. It is also analogous to electrical staging (i.e. segmented electrodes) and hydraulic staging (i.e. varied number of membrane pairs) for varying the voltage and flow rate respectively in the same ED stack [39]. Because time-variant ED batch operation is able maintain applied current density near limiting and fully utilize an available power source for maximized water production rate, ED systems designed with this technology may result in reduced capital costs compared to static, continuous ED systems composed of multi-stage ED stacks or multiple ED stacks in series. The hardware required to make a time-variant ED system is readily available off-the-shelf, with some components (e.g. conductivity sensors) already routinely included in conventional ED batch systems.

Section 5.3 reveals a trade-off between power consumption and desalination rate. Flexible operation allows ED systems to utilize much higher levels of power compared to a similarly sized static ED system, which

will increase desalination rate but result in higher SEC. The additional energy consumption of the accelerated production rate may not be an issue in some applications in which operational time is critical, or available energy is abundant (e.g. solar irradiance at mid-day). To be economically viable therefore, the cost of energy provided by either on-grid or off-grid sources should be low enough to justify the additional energy consumption required to operate time-variant ED systems at the high flow rates required for maximizing desalination rate. For on-grid cases, operation costs could be reduced while maximizing production rate by either limiting the overall system power threshold and/or the pumping power threshold.

To justify higher SEC in on-grid applications, time-variant ED technology could utilize variable electricity tariffs between peak and off-peak times, which are part of a demand response (DR) approach for reducing peak loads [40]. Various DR programs provide financial benefits to customers who are willing to shift loads from peak times to off-peak times. Wang and Li [16] surveyed time-of-use pricing services in the US and found that peak time prices can be 500-600% higher than off-peak time prices in summer months (June-September), and 30%-200% higher in other months. Such considerable price differences could incentivize the adoption of time-variant ED systems to produce more water, or produce water at a faster rate during off-peak periods, than existing technologies, which could potentially reduce overall water costs. Time-variant ED systems could also facilitate the integration of renewable energy sources into the electrical grid by providing a consumer of excess energy production on an irregular schedule, thereby reducing carbon emissions from energy sources currently used to meet peak demands (e.g. coal and natural gas).

For off-grid applications, time-variant operation could enable ED systems to directly utilize all available intermittent renewable energy, such as peak midday solar irradience that would otherwise be neglected or stored in batteries. This could significantly reduce system capital costs by reducing the battery capacity required for renewable energy peak shifting. Small battery capacity and high water production rates would be particularly valuable for disaster response applications, where small-scale, lightweight, PV-powered time-variant ED systems could be rapidly shipped and deployed. For microgrid solar systems, which are gaining popularity in cost-constrained, remote communities in developing countries [41], time-variant ED systems could reduce electricity costs by utilizing otherwise unused solar energy and creating additional value through the production of potable water.

7. Conclusions

This paper proposes a highly-flexible and production-optimized ED desalination technology for brackish water with two degrees of freedom of control: applied ED stack voltage and pumping flow rate. This control method can enable flexible and effective uses of variable power sources on a timescale of seconds to maximize water production, which has particular value in utilizing renewables (e.g. wind and solar). Additionally, time-variant ED operation can improve utilization of membrane area by maximizing the applied current density, which could facilitate smaller and lower-cost desalination systems to hit a target production volume, compared to what can be achieved with static ED operation.

A pilot-scale, time-variant ED system was designed and built to validate the theory presented in this work. The time-variant system was able to utilize up to ~3 more power than if operated at static voltage and flow rate, achieving up to 45% greater desalination rates. Within the operational domain, the pilot system was shown to successfully operate at three different power inputs, successfully adjusting voltage and flow rate as anticipated. A trade-off between SEC and desalination rate was identified; in the three tests with different power levels, desalination rate was increased by 29%, 20% and 19% by using 62%, 52% and 30% more energy, respectively, compared to static ED batch operation.

For on-grid applications, time-variant ED operation could enable water producers to align production time and power consumption favorably with energy tariffs, which are lower in the evening. For off-grid systems, time-variant ED could remove or reduce the need for batteries (and their associated costs) by producing water when energy is available. The technology presented herein may enable engineers to design brackish water ED desalination systems for new applications, smaller size scales, and at lower costs than what can be achieved with current technology. As a result, time-variant ED may have particular value as a potable water source for poor, off-grid communities in developing countries.

Acknowledgements

This work was supported by the US Bureau of Reclamation DWPR program (R17AC00150, R18AC00109), Tata Projects Ltd., Xylem Water Solutions and Water Technology, and the MIT Energy Initiative. We would like to thank Randall Shaw, Dan Lucero, and Francisco Nisino at BGNDRF for their technical support. We would like to thank Elizabeth Brownell, Natasha

C. Wright, Rashed Al-Rashed, Sahil R. Shah, and Sandra L. Walter for building the pilot system presented in this work at BGNDRF, and for their fruitful discussions about this research. I.M.P, and T.B acknowledge the support from Singapore's National Research Foundation through the Singapore-MIT Alliance for Research and Technology's 'Low energy electronic systems (LEES) IRG'. W.H. acknowledges the support from the Royal Academy of Engineering Research (RAEng) Engineering Research for Development Fellowship to complete this manuscript.

8. Reference

[1] M. M. Mekonnen, A. Y. Hoekstra, Four billion people facing severe water scarcity, Science advances 2 (2) (2016) e1500323.

[2] W. B. Group, High and dry: Climate change, water, and the economy, World Bank, 2016.

[3] J. S. Stanton, D. W. Anning, C. J. Brown, R. B. Moore, V. L. McGuire, S. L. Qi, A. C. Harris, K. F. Dennehy, P. B. McMahon, J. R. Degnan, et al., Brackish groundwater in the united states, Tech. rep., US Geological Survey (2017).

[4] SAO India, ground water quality in shallow aquifer of India, Available at https://www.indiastat.com/table/villages/6376/ruralfacilities/281388/281420/data.aspx (2018/08/23).

[5] Groundwater in china: Part 1 - occurance and use, Available at https://ecoinnovation.dk/media/mst/94641/130618%20Groundwater%20in%20China_Part%201_Occurrence%20and%20Use.pdf (2019/08/23).

[6] B. D. Negewo, Renewable energy desalination: an emerging solution to close the water gap in the Middle East and North Africa, World Bank Publications, 2012.

[7] N. Ghaffour, J. Bundschuh, H. Mahmoudi, M. F. Goosen, Renewable energy-driven desalination technologies: A comprehensive review on challenges and potential applications of integrated systems, Desalination 356 (2015) 94–114.

[8] N. C. Wright, et al., Justification for community-scale photovoltaic-powered electrodialysis desalination systems for inland rural villages in india, Desalination 352 (2014) 82–91.

[9] A. Campione, L. Gurreri, M. Ciofalo, G. Micale, A. Tamburini, A. Cipollina, Electrodialysis for water desalination: A critical assessment of recent developments on process fundamentals, models and applications, Desalination 434 (2018) 121–160.

[10] M. Shatat, M. Worall, S. Riffat, Opportunities for solar water desalination worldwide, Sustainable cities and society 9 (2013) 67–80.

[11] M. S. Miranda, D. Infield, A wind-powered seawater reverse-osmosis system without batteries, Desalination 153 (1-3) (2003) 9–16.

[12] W. He, S. Amrose, N. C. Wright, T. Buonassisi, I. M. Peters, A. G. Winter, Field demonstration of a cost-optimized solar powered electrodialysis reversal desalination system, Desalination, submitted.

[13] D. W. Bian, S. M. Watson, N. C. Wright, S. R. Shah, T. Buonassisi, D. Ramanujan, I. M. Peters, et al., Optimization and design of a low-cost, village-scale, photovoltaic-powered, electrodialysis reversal desalination system for rural india, Desalination 452 (2019) 265–278.

[14] M. S. Ziegler, J. M. Mueller, G. D. Pereira, J. Song, M. Ferrara, Y.-M. Chiang, J. E. Trancik, Storage requirements and costs of shaping renewable energy toward grid decarbonization, Joule 3 (9) (2019) 2134–2153.

[15] H. Safaei, D. W. Keith, How much bulk energy storage is needed to decarbonize electricity?, Energy & Environmental Science 8 (12) (2015) 3409–3417.

[16] Y. Wang, L. Li, Time-of-use electricity pricing for industrial customers: A survey of us utilities, Applied Energy 149 (2015) 89–103.

[17] B. S. Richards, G. L. Park, T. Pietzsch, A. I. Schäfer, Renewable energy powered membrane technology: Safe operating window of a brackish water desalination system, Journal of membrane science 468 (2014) 400–409.

[18] G. L. Park, A. I. Schäfer, B. S. Richards, Renewable energy powered membrane technology: The effect of wind speed fluctuations on the performance of a wind-powered membrane system for brackish water desalination, Journal of Membrane Science 370 (1-2) (2011) 34–44.

[19] J. Shen, A. Jeihanipour, B. S. Richards, A. I. Schäfer, Renewable energy powered membrane technology: Experimental investigation of system performance with variable module size and fluctuating energy, Separation and Purification Technology 221 (2019) 64–73.

[20] B. S. Richards, D. P. Capão, W. G. Früh, A. I. Schäfer, Renewable energy powered membrane technology: Impact of solar irradiance fluctuations on performance of a brackish water reverse osmosis system, Separation and Purification Technology 156 (2015) 379–390.

[21] P. Malek, J. Ortiz, H. Schulte-Herbrüggen, Decentralized desalination of brackish water using an electrodialysis system directly powered by wind energy, Desalination 377 (2016) 54–64.

[22] F. Cirez, J. Uche, A. Bayod, A. Martinez, Batch ED fed by a PV unit: a reliable, flexible, and sustainable integration, Desalination and Water Treatment 51 (4-6) (2013) 673–685.

[23] P. Malek, Clean water from clean energy: removal of dissolved contaminants from brackish groundwater using wind energy powered electrodialysis, Ph.D. thesis, The University of Edinburgh (2015).

[24] J. M. Veza, B. Peñate, F. Castellano, Electrodialysis desalination designed for wind energy (on-grid tests), Desalination 141 (1) (2001) 53–61.

[25] J. Veza, B. Peñate, F. Castellano, Electrodialysis desalination designed for off-grid wind energy, Desalination 160 (3) (2004) 211–221.

[26] H. Xu, X. Ji, L. Wang, J. Huang, J. Han, Y. Wang, Performance study on a small-scale photovoltaic electrodialysis system for desalination, Renewable Energy.

[27] A. Campione, A. Cipollina, F. Calise, A. Tamburini, M. Galluzzo, G. Micale, Coupling electrodialysis desalination with photovoltaic and wind energy systems for energy storage: Dynamic simulations and control strategy, Energy Conversion and Management 216 (2020) 112940.

[28] S. R. Shah, S. L. Walter, et al., Using feed-forward voltage-control to increase the ion removal rate during batch electrodialysis desalination of brackish water, Desalination 457 (2019) 62–74.

[29] Y. Tanaka, A computer simulation of feed and bleed ion exchange membrane electrodialysis for desalination of saline water, Desalination 254 (1-3) (2010) 99–107.

[30] Y. Tanaka, Development of a computer simulation program of feed-and-bleed ion-exchange membrane electrodialysis for saline water desalination, Desalination 342 (2014) 126–138.

[31] S. R. Shah, N. C. Wright, P. A. Nepsky, A. G. Winter, Cost-optimal design of a batch electrodialysis system for domestic desalination of brackish groundwater, Desalination 443 (2018) 198–211.

[32] V. V. Nikonenko, A. V. Kovalenko, M. K. Urtenov, N. D. Pismenskaya, J. Han, P. Sistat, G. Pourcelly, Desalination at overlimiting currents: State-of-the-art and perspectives, Desalination 342 (2014) 85–106.
[33] N. C. Wright, S. R. Shah, S. E. Amrose, A. G. Winter, A robust model of brackish water electrodialysis desalination with experimental comparison at different size scales, Desalination 443 (2018) 27–43.
[34] M. Šavar, H. Kozmar, I. Sutlović, Improving centrifugal pump efficiency by impeller trimming, Desalination 249 (2) (2009) 654–659.
[35] Y. Zhang, L. Pinoy, B. Meesschaert, B. Van der Bruggen, A natural driven membrane process for brackish and wastewater treatment: photovoltaic powered ed and fo hybrid system, Environmental science & technology 47 (18) (2013) 10548–10555.
[36] SUEZ Water Technologies & Solutions, Welcome To Document Library (Accessed on September 2020).
[37] R. P. Allison, Electrodialysis reversal in water reuse applications, Desalination 103 (1-2) (1995) 11–18.
[38] H. Strathmann, Electrodialysis, a mature technology with a multitude of new applications, Desalination 264 (3) (2010) 268–288.
[39] N. C. Wright, A. G. Winter, Village-scale electrodialysis desalination: Field trial validation, in: International Design Engineering Technical Conferences and Computers and Information in Engineering Conference, Vol. 58134, American Society of Mechanical Engineers, 2017, p. V02BT03A019.
[40] M. H. Albadi, E. F. El-Saadany, A summary of demand response in electricity markets, Electric power systems research 78 (11) (2008) 1989–1996.
[41] Tata power launches TP renewable microgrid supported by the Rockefeller Foundation, `https://www.tatapower.com/products-and-services/micro-grids.aspx`.
[42] K. M. Chehayeb, D. M. Farhat, K. G. Nayar, et al., Optimal design and operation of electrodialysis for brackish-water desalination and for high-salinity brine concentration, Desalination 420 (2017) 167–182.
[43] H.-J. Lee, F. Sarfert, H. Strathmann, S.-H. Moon, Designing of an electrodialysis desalination plant, Desalination 142 (3) (2002) 267–286.
[44] Y. Tanaka, A computer simulation of batch ion exchange membrane electrodialysis for desalination of saline water, Desalination 249 (3) (2009) 1039–1047.
[45] Y. Kim, W. S. Walker, D. F. Lawler, Electrodialysis with spacers: effects of variation and correlation of boundary layer thickness, Desalination 274 (1-3) (2011) 54–63.

9. Appendix

9.1. Appendix A: hydraulic diameter and the Sherwood number

In the mass transfer coefficient k, the hydraulic diameter d_h is

$$d_h = \frac{4\epsilon}{2/h + (1-\epsilon)(8/h)}, \tag{19}$$

where ϵ is the void fraction. The Sherwood Number, a measure of mass transfer performance, is correlated to the Reynolds Number and the Schmidt number by

$$Sh = aRe^b Sc^c. \tag{20}$$

The Schmidt number Sc is a material dependent, non-dimensional quantity relating the momentum and mass diffusion. The Reynolds number is a dimensionless number relating inertial to viscous stresses in the flow. They are

$$Sc = \frac{\mu}{\rho_{aq} D_{aq}} \tag{21}$$

and

$$Re = \frac{\rho_{aq} u_{ch} d_h}{\mu}. \tag{22}$$

9.2. Appendix B: The pump curve used in this paper

Two pumps were used in the ED system presented: a diluate pump and a concentrate pump. The two pumps were the same model, but the performance slightly varied due to differences in their associated hydraulic circuits in the ED system. In order to mitigate the fouling, electrodialysis reversal (EDR) operation was used during testing, such that the polarity of the electrical field was reversed after each batch. As a result, each pump operated in two positions, namely position 1 and position 2. Figure 10 presents the experimentally measured pump curves, which were used to predict pump performance in this work.

9.3. Appendix C: Desalination rate of CVCQ at different flow rates

An appropriate flow velocity is determined by the trade-off between pumping power and ED stack power consumption, which is expected to be small enough to reduce pumping power, but just high enough to increase the limiting current density and to limit concentration polarization [42]. Consequently, the flow rate of a conventional ED batch is usually between 4–10 cm/s in each membrane channel according to prior experimental and theoretical studies [43, 44, 45], and the manufacture's recommended flow rate of (~7 cm/s) [33]. Therefore, Fig. 11 presents the desalination performance of static ED operation with several flow rates for potential comparisons.

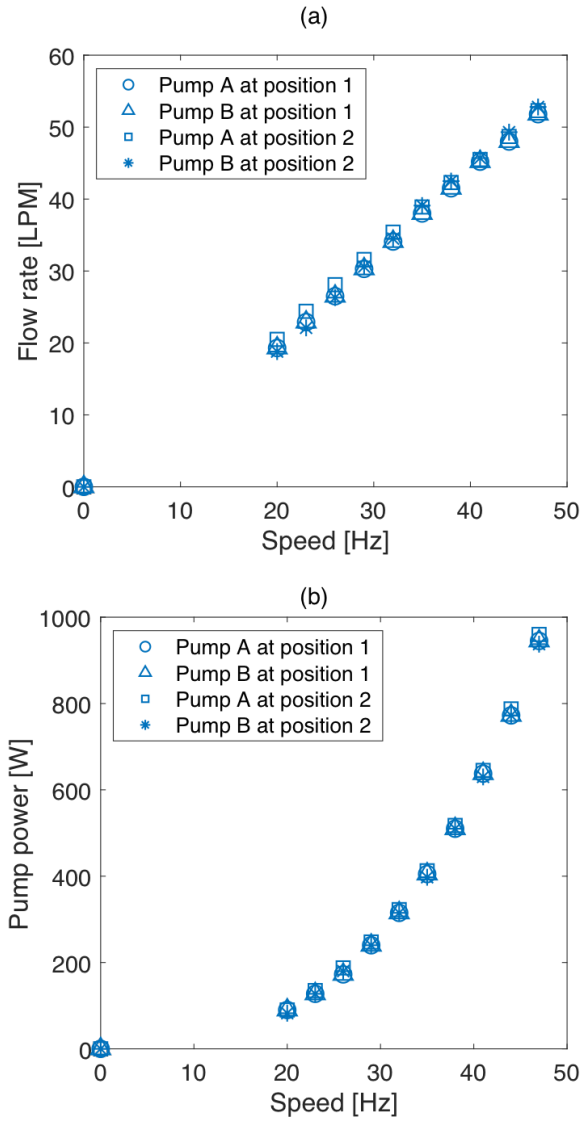

Figure 10: Pumps curves of the two pumps used in the pilot time-variant ED system.

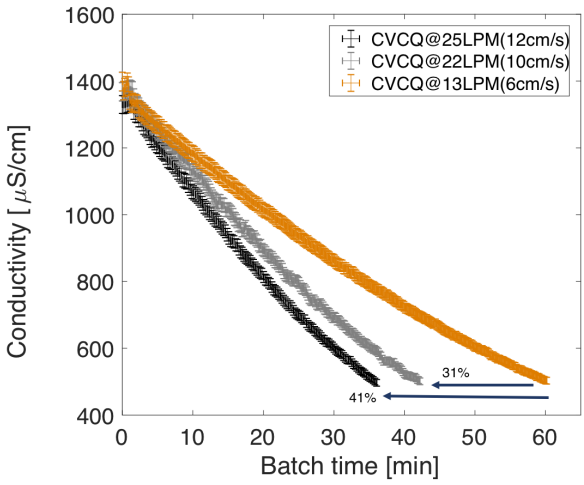

Figure 11: The diluate conductivity versus the batch time of CVCQ operation at various flow rates.

Acronyms

AEM Anion exchange membranes.

BGNDRF Brackish Groundwater National Desalination Research Facility.

CapEx Captial expenditure.

CEM cation exchange membranes.

CVCQ Constant voltage constant flow rate.

DC Direct current.

DR Demand response.

ED Electrodialysis.

OpEx Operational expenditure.

PLC Programmable logic controller.

PV Photovoltaic.

RO Reverse osmosis.

SEC Specific energy consumption.

TDS Total dissolved solids.

VFD Variable frequency drive.

VVCQ Variable voltage constant flow rate.

VVVQ Variable voltage variable flow rate.

Symbols

A Membrane area, m^2

C_c^b Bulk concentration of concentrate, mol m^{-3}

C_d^b Bulk concentration of diluate, mol m^{-3}

d_h Hydraulic diameter, m

D Diffusion coefficient, $m^2\ s^{-1}$

F Faraday constant, 96485 C mol^{-1}

H Pump head, m

i Current density, A m^{-2}

I Current, A

k Mass transfer coefficient, m s^{-1}

L Membrane channel length, m

N Number of cell pairs

P Power, W

Q_c Flow rate of concentrate, $m^3\ s^{-1}$

Q_d Flow rate of diluate, $m^3\ s^{-1}$

r_i Safety factor

R Resistance, Ω

Sh Sherwood Number

t Time, s

T Temperature, K

$t^{AEM,CEM}$ Transport numbers of the AEM and CEM membranes

$t^{+,-}$ Minimum of the anion and cation transport numbers

V_{el} Electrode potential, V

V Voltage, V

V^{cell} Volume of a cell, m^3

V^{tank} Volume of tank, m^3

W Stack width, m

z Ion charge

ϕ_A Open-area porosity of the spacer

ϕ Current leakage factor

τ Control time, s

Superscript and subscript

0 Position in the tank

AEM Anion exchange membrane

CEM Cation exchange membrane

y Position at the segment y

Y Position at the segment Y

τ_i Control time step i